Supporting Information

Enhanced Activity and Durability of Ir Single Atom Catalyst for Electrocatalytic Oxygen Evolution Reaction Through Synergistic Electronic Coupling with Co_3O_4 Matrix

Astha Gupta[a], Swarup Ghosh[b], Dinesh Bhalothia[c*], Joydeep Chowdhury[d], and Surojit Pande[a*]

[a]Department of Chemistry, Birla Institute of Technology and Science, Pilani, Rajasthan-333031, India

Corresponding author: Surojit Pande, E-mail: spande@pilani.bits-pilani.ac.in

[b]School of Computer Science and Artificial Intelligence, SR University, Warangal, Telangana 506371, India.

[c]Department of Electronics and Communication Engineering, Manipal University Jaipur, Rajasthan 303007, India

[d]Department of Physics, Jadavpur University, 188, Raja S.C. Mallick Road, Kolkata, 700032, India.

Characterization of material: Powder X-ray diffraction (PXRD) was done using the Rikagu Mini Flex II diffractometer having incident radiation of Cu Kα. The data was recorded at 2º per min scan rate, from 20º to 60º for all the bare and doped samples. The morphology of the pristine Co_3O_4 and Ir_{SAC}-Co_3O_4 material was inspected by field emission scanning electron microscopy (FESEM) instrument, model-"APREO S", XT microscope. Morphology, lattice spacing, and crystallinity were further examined with Field emission transmission electron microscope (FE-TEM, JEM-2100F). For TEM analysis, the samples were collected from carbon cloth via sonication and drop casted on a carbon-coated Cu grid and dried in a vacuum chamber. X-ray photoelectron spectroscopy (XPS) was performed with Omicron EA 125 source using Al Kα radiation having energy 1486.7 eV. Throughout the XPS analysis, base pressure was sustained < 10^{-9} m bar in the UHV. The HAADF-STEM images were collected at the National Sun Yat-sen University, Taiwan. The preparation of STEM samples began with dispersing the catalyst powder in isopropanol (IPA) through ultrasonication. This dispersion was then drop-cast onto 200 mesh copper grids. Afterward, the specimens were dried at 120°C for 48 hours in an oven. Before loading the samples into the TEM chamber, they were cleaned with plasma to remove any surface contaminants. As a reference, the binding energy peak at 284.5 eV of C 1s was used to detect any kind of variation. For electrochemical water splitting application, the CH instrument (CHI604E) was used. ICP analysis was done with model Perkin Elmer AVIO ICP spectrometer.

X-ray Absorption Spectroscopy (XAS) measurements, including X-ray Near-Edge Structure (XANES) and Extended X-ray Absorption Fine Structure (EXAFS), were performed at the Ir L_3-edge (11,207 eV) and Co K-edge (7709 eV) at room temperature. Ir L_3-edge XAS measurements were carried out at BL-17C of the National Synchrotron Radiation Research Center (NSRRC), Hsinchu, Taiwan in fluorescence mode using a multi-element solid-state detector to collect high-quality spectra for dilute samples. Energy calibration was performed simultaneously with an Ir metal foil reference. Co K-edge XAS measurements were performed at the Energy Scanning EXAFS beamline (BL-9) of the Indus-2 Synchrotron Source (2.5 GeV, 120 mA) at the Raja Ramanna Centre for Advanced Technology (RRCAT), Indore, India. The beamline optics consist of a Rh/Pt-coated meridional cylindrical mirror for collimation, a Si (111) DCM for energy selection, and sagittal focusing of the second crystal for horizontal beam focusing. An additional Rh/Pt-coated bendable mirror provides vertical focusing at the sample position. During measurements, the second crystal was detuned by ~60% to minimize higher-order harmonics. Data

were collected in both transmission and fluorescence modes, using ionization chambers filled with N_2, He, and Ar depending on the edge and measurement mode. A Co metal foil was simultaneously measured for energy calibration. For both edges, samples were prepared by mixing the required amount of catalyst with cellulose and pressing into 1 mm thick pellets under a pressure of 2 tons to achieve an appropriate edge jump. Standard procedures for normalization and background subtraction were performed using ATHENA software (version 0.9.26).[1] Fourier transforms (FT) of the EXAFS oscillations were obtained to generate $|\chi(R)|$ versus R space spectra, and quantitative fitting was carried out using ARTEMIS software (version 0.9.26), with theoretical scattering paths calculated by FEFF6 and structural models generated by the ATOMS code.[2] EPR measurements were recorded using the Bruker A300-9.5/12/S/W at room temperature.

Calculation Method

Electrochemical calculation:

The calculation of catalyst loading and mass activity of the electrocatalysts on carbon cloth was carried out using the following equations 1 and 2, respectively.

$$M_{catalyst} = [Weight_{(catalyst\ loaded\ CC)} - Weight_{(Bare\ CC)}] / area\ (cm^2) \quad [1]$$

$$Mass\ activity = observed\ current\ density\ at\ a\ fixed\ potential/catalyst\ loading \quad [2]$$

As a result, catalyst loading on carbon cloth was 0.28 mg on a 0.16 cm^2 area. Mass activity (A/g) for OER was calculated by using the observed current density at a fixed potential of 1.55 V *vs.* RHE. To calculate the electrochemical surface-active area (ECSA) for OER, CV analysis was carried out at different scan rates and a fixed potential of 1.125 V *vs.* RHE, the observed current was plotted against the scan rate. The slope of the observed straight line is the double-layer capacitance (C_{dl}), which is directly proportional to ECSA. To calculate the roughness factor, the ECSA of that electrode was divided by geometric area.

Tafel slope calculation, $\eta = a + b\log j$, where, "η" is the overpotential, "j" is the current density and "b" is the Tafel slope.

Turn over frequency (TOF) calculation:

While calculating the TOF, it is assumed that all the metal atoms on the catalyst/electrode surface are taking part/active in the electrocatalysis. The following formula is used to calculate the TOF:

$$TOF = j \times A / 4 \times F \times n \quad (3)$$

Where:

j = current density at a fixed potential

A = geometric area

F = Faraday's con. (96485.3 C/ mol)

n = the moles of metal atoms present on the electrode surface

(The value of n is calculated from the molecular weight of the compound and the amount of catalyst present on the electrode surface.)

Preparation of standard electrocatalyst for OER:

For the standard catalyst of OER, IrO_2 was used. The same amount of catalyst (0.28 mg) was used to compare the electrocatalytic activity. In a small glass vial, 0.28 mg of IrO_2 was taken along with 200 μL of isopropyl alcohol and 20 μL of Nafion (an adhesive), and the mixture was sonicated for 30 min. After that, the whole mixture was transferred quantitatively into 0.4 × 0.4 cm^2 CC and was used.

Chemicals

Cobalt(II)nitrate hexahydrate and urea were purchased from Merck, India and KOH was purchased from SRL, India. Iridium(III)chloride hydrate was purchased from Sigma Aldrich. Carbon cloth (CC), the conducting substrate, was purchased from Shree Balaji Scientific Company, India. To clean the CC, it was first soaked in concentrated nitric acid for 12 h and then rinsed in deionized water. The final procedure was drying the washed CC in a standard oven at 50 °C for a few hours after cleaning it with Milli-Q water, ethanol, and acetone. Except for CC, none of the chemicals were purified.

Computational details

The Quantum ESPRESSO (QE) software suite was used to carried out the first-principles density (DFT) calculations.[3-5] The X-ray powder diffraction data as obtained from our experimental observation have been primarily considered to model the crystal structure of Co_3O_4 compound. The Ir-SAC Co_3O_4 system is formed by doping a single Ir atom by substituting a Co atom in the Co_3O_4 crystal. The geometry optimization of the crystal structures has been performed by simultaneously varying the crystallographic axes and atomic positions under Broyden-Fletcher-Goldfarb-Shanno (BFGS) scheme. [6-9] The valence electron configuration for Co, O and Ir atoms are $4s^23d^7$, $2s^22p^4$, and $5d^76s^24p^5$ respectively which are recognized as plane-wave whose kinetic energy cut-off was set at 70 Ry. The electron-ion interactions was included in the systems through the projector augmented wave (PAW) pseudopotentials [10]. The Perdew-Burke-Ernzerhof (PBE) functional, which is a parametric version of the generalized gradient approximation (GGA) used to define the exchange-correlation (XC) term of the pseudopotential.[11] The convergence requirement for total electronic energy was set at 10−8 a.u., with a maximum Hellman-Feynman force threshold of 10^{-3} a.u. To optimize geometry and calculate self-consistent field (SCF) energy, a 10×10×10 gamma-centered k-point mesh with the Monkhorst-pack scheme was used initially.

The defect formation energy (ΔE) of Ir_{SAC}-Co_3O_4 has been evaluated using the following mathematical expression. [12-14].

$$\Delta E = \frac{1}{N_{Ir}}[E_{SAC} - E_{bare} - N_{Ir}(\mu_{Ir} - \mu_{Co})] \quad \text{(S1)}$$

where E_{SAC} and E_{bare} represent total energies of Ir_{SAC}-Co_3O_4 and Co_3O_4 systems, N_{Ir}=1 is the number of single atom dopant Ir, μ_{Ir} and μ_{Co} denote the chemical potentials of the single Ir and Co atoms, respectively. The chemical potentials μ_{Ir} and μ_{Co} were computed to their respective bulk phases, i.e., face-centered cubic metallic Ir and hexagonal close-packed metallic Co, which corresponds to the metal-rich limit. This choice is consistent with established defect energetics protocols for transition-metal oxides, ensuring that the calculated energies remain thermodynamically bounded [15, 16]. Under O-rich conditions, the chemical potential would be referenced to half the energy of an O_2 molecule; however, such a choice would only shift the absolute values of ΔE and would not affect the relative stability trend between tetrahedral and octahedral substitution sites of Co, since both are evaluated within the same thermodynamic framework.

The electronic band structures of Co_3O_4 and Ir_{SAC}-Co_3O_4 compounds were calculated along $\Gamma \rightarrow X \rightarrow W \rightarrow L$ high-symmetry order where each high-symmetry point consists of 80 k–point mesh. The electronic band gap (E_g) values of the studied systems have been computed from the Heyd-Scuseria-Ernzerhof (HSE) functional with the aid of screening parameter 0.20 [17]. A dense k – point grid of 20×20×20 mesh was further considered for density of states (DOS) and orbital resolved projected density of states (PDOS) calculations. The route for electrochemical of OER in pristine and SAC material were assessed using the QE software's climbing image nudged elastic band (CINEB) approach.

Table S1: ICP-AES analysis of Ir decorated Co_3O_4 samples by using different con. of $IrCl_3$ sol.

Con. of $IrCl_3$ sol. used	**wt% of Ir in Ir/Co_3O_4 samples**
5 mg/mL	2.56
10 mg/mL	3.02
15 mg/mL	3.74
20 mg/mL	4.72
25 mg/mL	4.91

Table S2: Atomic % obtained from SEM-EDS mapping analysis of Ir/CO_3O_4 samples synthesized by using different concentration of $IrCl_3$

Con. of $IrCl_3$ sol.	**5 mg/mL**	**10 mg/mL**	**15 mg/mL**	**25 mg/mL**
Element	Atomic %	Atomic %	Atomic %	Atomic %
C	27.85	29.77	30.65	34.85
O	24.55	37.04	21.43	17.51
Co	47.49	41.92	46.67	46.01
Ir	0.11	1.06	1.25	1.90
Total	100.00	100.00	100.00	100.00

Table S3: XAS determined quantitative structural parameters of the Ir_{SAC}-Co_3O_4 and control samples.

Samples	Ir L_3 Edge			Co K-edge		
	bond pair	CN	R	bond pair	CN	R
Ir-CO_3O_4	Ir-Ir	N/A	N/A	Co-Co	4.68	2.932
	Ir-O	3.01	2.912	Co-O	1.36	2.925
	Ir-Co	2.16	2.986	Co-Ir	N/A	N/A
CO_3O_4	N/A			Co-Co	4.56	2.933
				Co-O	2.45	2.926

*the Debye-Waller factor (σ^2) is determined to be 0.0035 $Å^2$ for fitting all experimental spectra.

Table S4: XPS binding energy values of Co_3O_4, and Ir_{SAC}-Co_3O_4 (pre and post electrocatalysis)

Binding energy (eV)	**Co_3O_4**	**Ir_{SAC}-Co_3O_4**	**Ir_{SAC}-Co_3O_4 (Post electrolysis)**
Co^{+2} ($2p_{3/2}$)	780.81	781.4	781.27
Co^{+3} ($2p_{3/2}$)	779.37	779.98	780.04
Co^{+2} ($2p_{1/2}$)	795.75	796.68	796.44
Co^{+3} ($2p_{1/2}$)	794.31	795.07	795.06
O1	529.52	530.28	530.22
O2	530.90	531.53	531.69
O3	532.24	532.48	533.23
Ir ($4f_{7/2}$)		62.39	62.33
Ir ($4f_{5/2}$)		65.19	65.18

Table S5. Electrochemical parameters of Ir/Co_3O_4 sample synthesized by using different concentration of $IrCl_3$ solution

Sample synthesized by using diff. con. of $IrCl_3$ sol.	**Onset potential@10 mA/cm^2**	**TOF(S^{-1}) at η_{370}**	**Mass activity at 1.55 V (A/g)**
Ir/Co_3O_4 (5 mg/mL)	1.543	0.02	166.75
Ir/Co_3O_4 (10 mg/mL)	1.514	0.03	274.28
Ir/Co_3O_4 (15 mg/mL)	1.531	0.026	220.25
Ir/Co_3O_4 (20 mg/mL)	1.541	0.021	165.48
Ir/Co_3O_4 (25 mg/mL)	1.544	0.021	142.06

Table S6: A benchmark table comparing the performance with the literature for OER

S. No.	Electrocatalyst	Electrolyte	Electrode Reaction	Overpotential to generate 10 mA/cm^2 current density	Tafel slope (mV/dec)	Stability	Ref
1.	0.5 wt% Pt/NiO	1 M KOH	OER	358 mV	33	-	18
2.	$Ir_{18wt\%}$ NiO	1 M KOH	OER	215 mV	38	10 h	19
3.	Ir_{SA}-V_o-$CoNiO_2$	1 M KOH	OER	183 mV	64.8	25 h	20
4.	Ir_{emb}-NiO	1 M KOH	OER	256 mV	41	25 h	21
5.	Ru/Co_3O_{4-x}	1 M KOH	OER	280 mV	86.9	150 h	22
6.	Ru/CoFe-LDHs	1 M KOH	OER	195 mV	39	25 h	23
7.	(Ir–$NiCo_2O_4$NSs	0.5 M H_2SO_4	OER	240 mV	60	70 h	24
8.	$Ir_{0.06}Co_{2.94}O_4$	0.1 M $HClO_4$	OER	220 mV	45	200 h	25
9.	Ir_1 Ni@MoO_2 SAAs	1 M KOH	OER	280 mV	91 mV/dec	100 h	26
10.	Ir/$NiFe_2O_4$	1 M KOH	OER	196 mV	36.85 mV/dec	400 h	27
11.	Ir–SAs@Ni aerogel	1 M KOH	OER	281 mV	64.36 mV/dec	~65 h	28
12.	Ir_{SAE}-CMO	0.5 M H_2SO_4	OER	235 mV	90 mV/dec	25 h	29
13.	Ir_1/Ni LDH-T	1 M KOH	OER	228 mV	41 mV/dec	60 h	30
14.	Ir-$_{SAC}$ Co_3O_4	1 M KOH	OER	270 mV	76	96 h	This work

Table S7: parameters obtained from electrochemical impedance spectroscopy (EIS) data for Pristine Co_3O_4, and Ir_{SAC}-Co_3O_4 sample

Electrode	**R_s (Ohm)**	**R_{CT} (Ohm)**	**C_{dl} (mF)**	**Frequency (Hz)**
Co_3O_4	7.12	12.19	0.013	0.1 to 5000
Ir_{SAC}-Co_3O_4	6.3	5.12	0.018	0.1 to 5000

Table S8: All OER parameters of Co_3O_4, and Ir_{SAC}-Co_3O_4 samples

Electrode	Potential (V) vs. RHE required to generate 10 mA/cm^2	Tafel slope (mV/dec)	ECSA (cm^2)	Mass Activity (A/g) at 1.55 V vs. RHE	R_f	R_s (Ohm)	R_{CT} (Ohm)	TOF (S^{-1}) at η_{370}
Co_3O_4	1.58 V	90	4.03	35.74	25.18	7.12	12.19	0.005
Ir-$_{SAC}$ Co_3O_4	1.514 V	76	12.63	274.28	78.75	6.3	5.12	0.03
IrO_2	1.64 V	121		35.71				0.002

Figure S1: XRD analysis of pristine Co_3O_4, and Ir_{SAC}-Co_3O_4

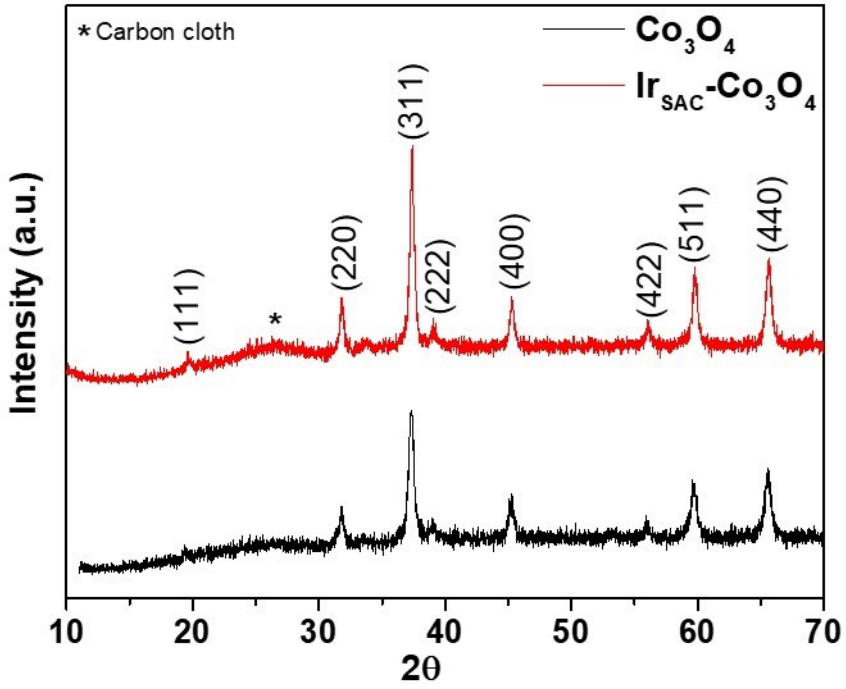

Figure S2 a and b: FESEM analysis of pristine Co_3O_4 sample at (a) low, (b) high magnification

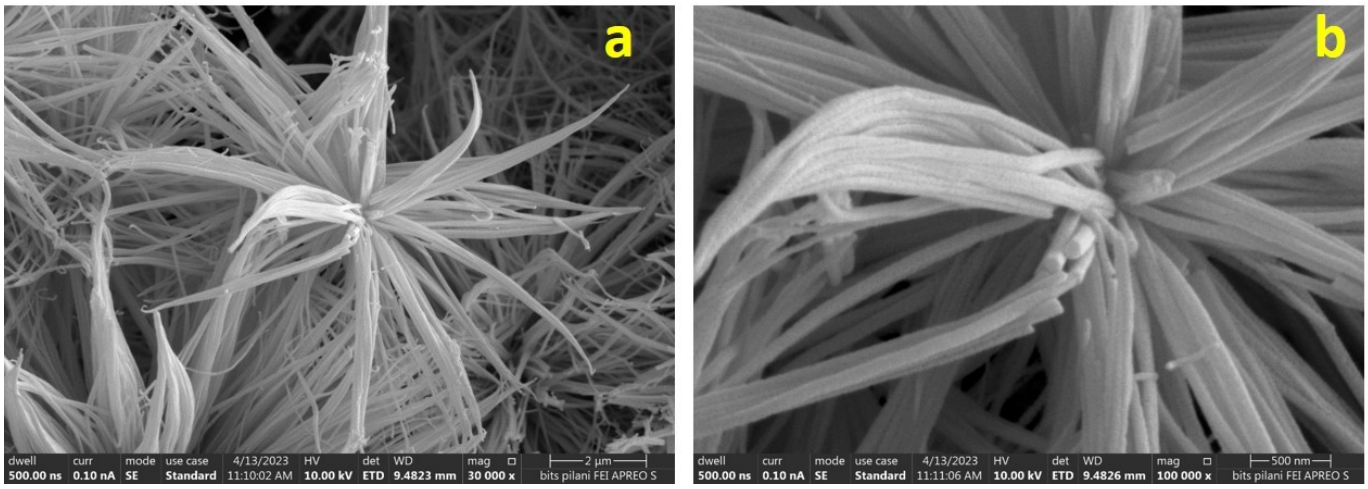

Figure S2 c-h: FESEM images of Ir_{SAC}-Co_3O_4 sample synthesized by using 5 mg/mL (c and d), 15 mg/mL (e and f), and 25 mg/mL (g and h) $IrCl_3$ solution.

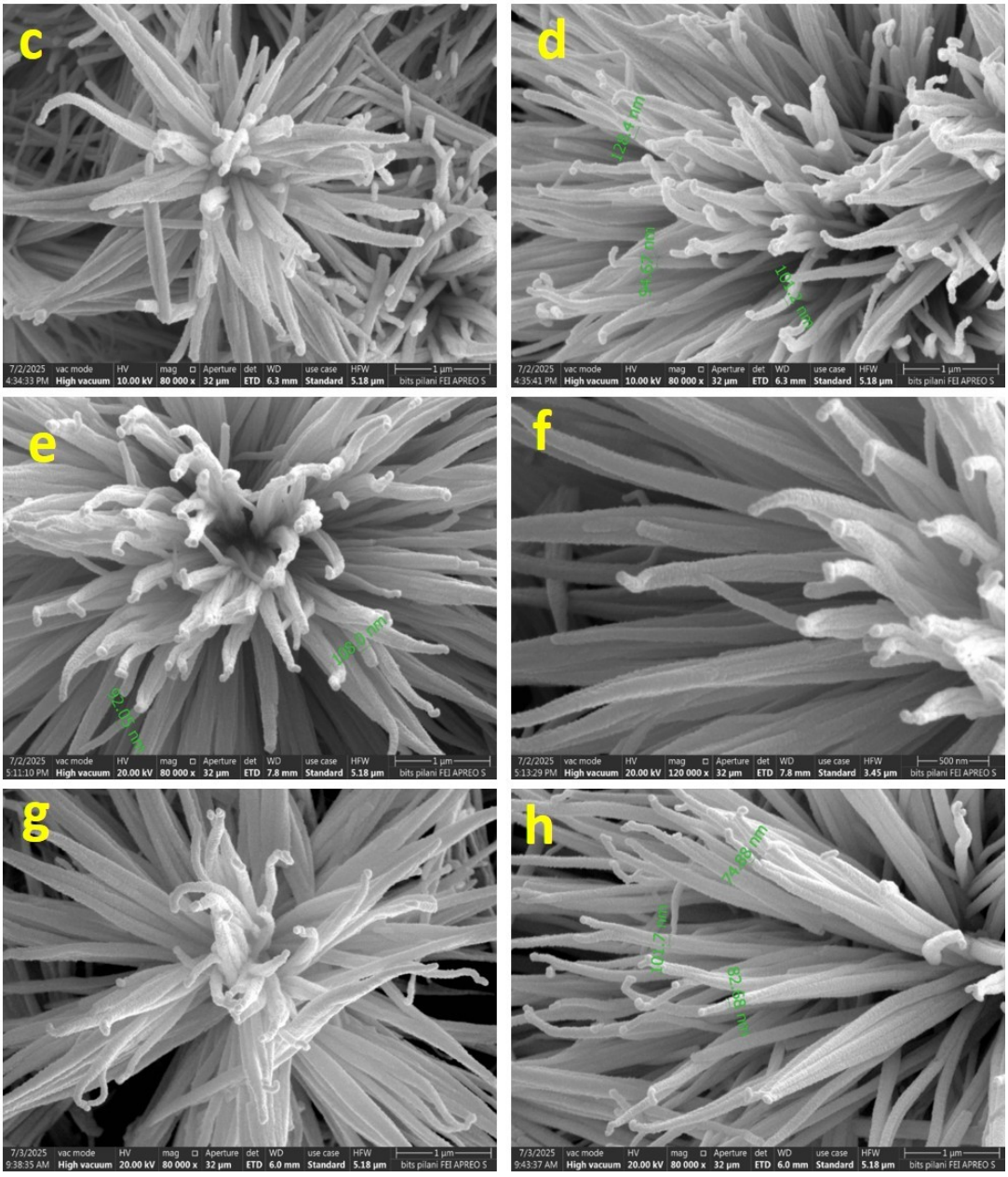

Figure S3: (a), (b) TEM, and (c) HRTEM analysis of pristine Co_3O_4, and TEM (d), and HRTEM

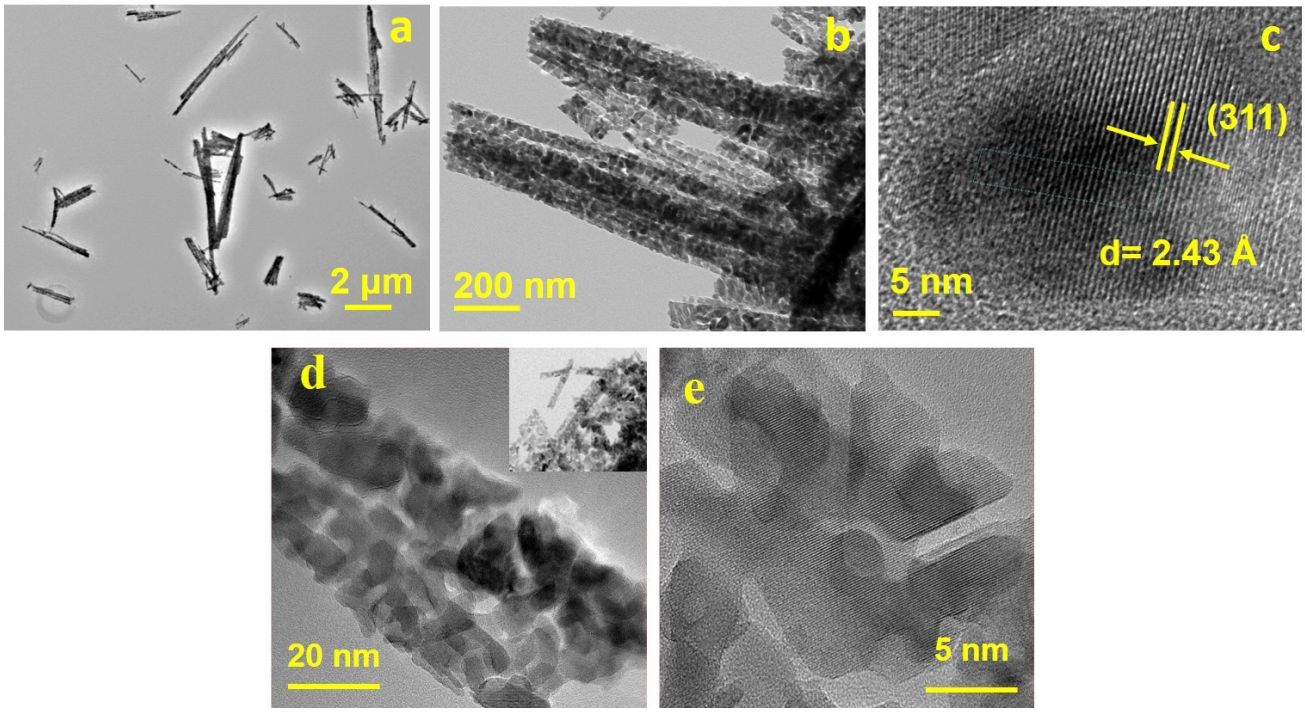

(e) images of Ir_{SAC}-Co_3O_4 samples (10 mg/mL).

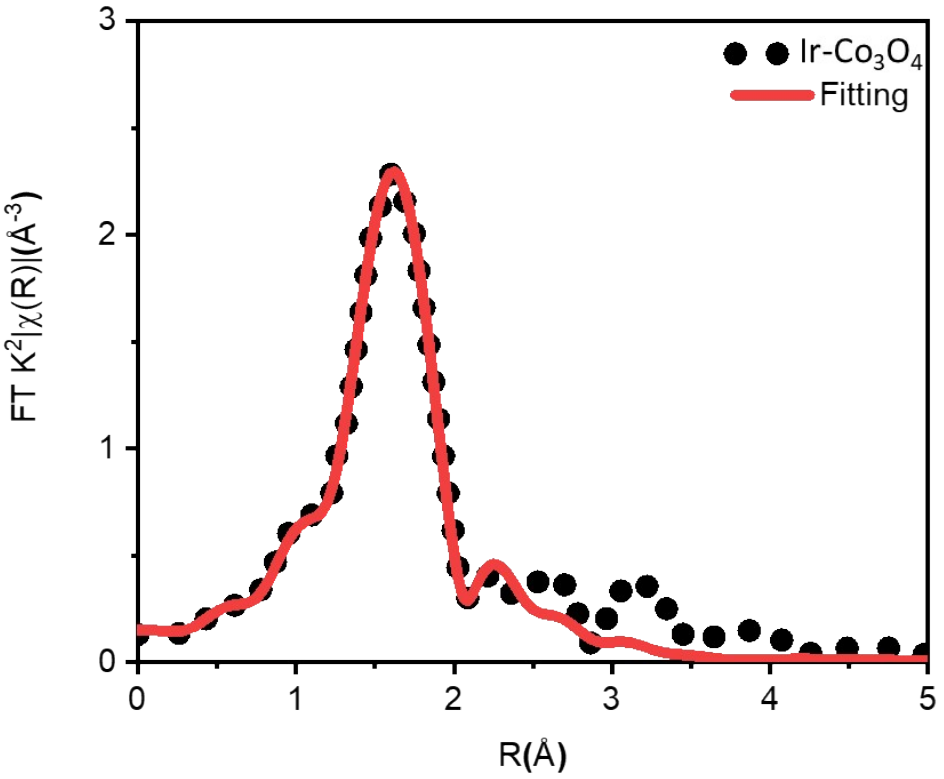

Figure S4a. The overlay spectra of Ir-Co_3O_4 EXAFS and corresponding fitting.

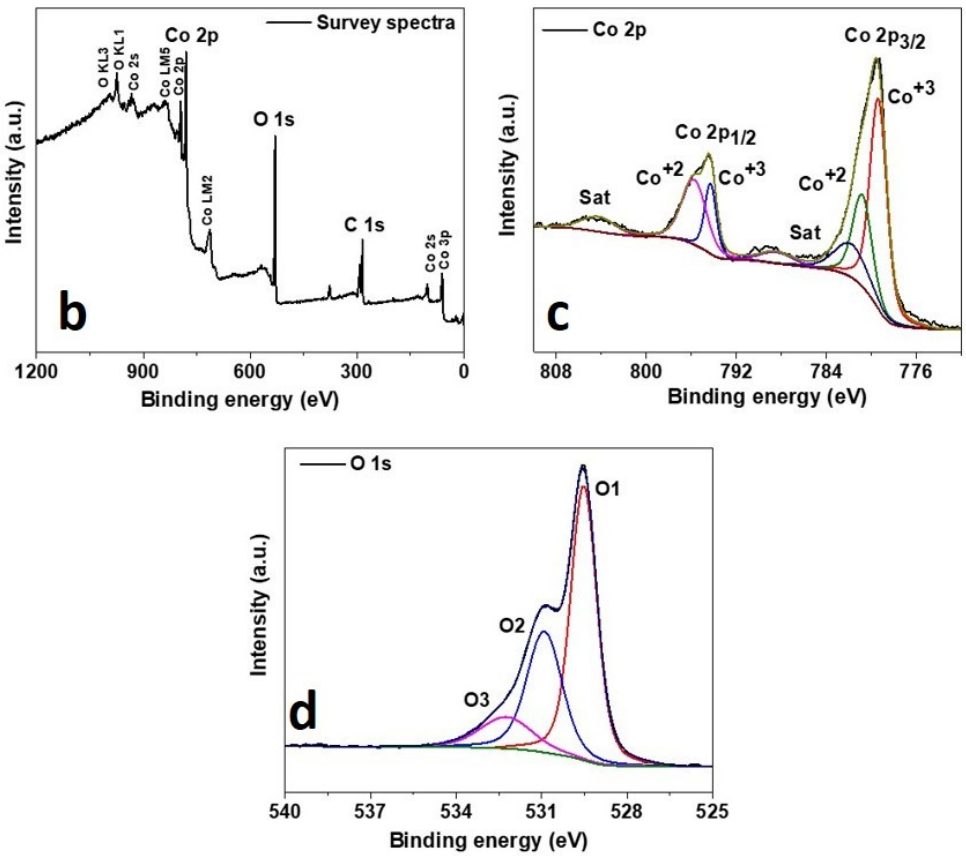

Figure S4: XPS analysis of Co_3O_4 (b) survey spectra, deconvoluted spectra of (c) Co 2p, and (d) O 1s

Figure S5: EPR analysis of Co_3O_4 and Ir_{SAC}-Co_3O_4

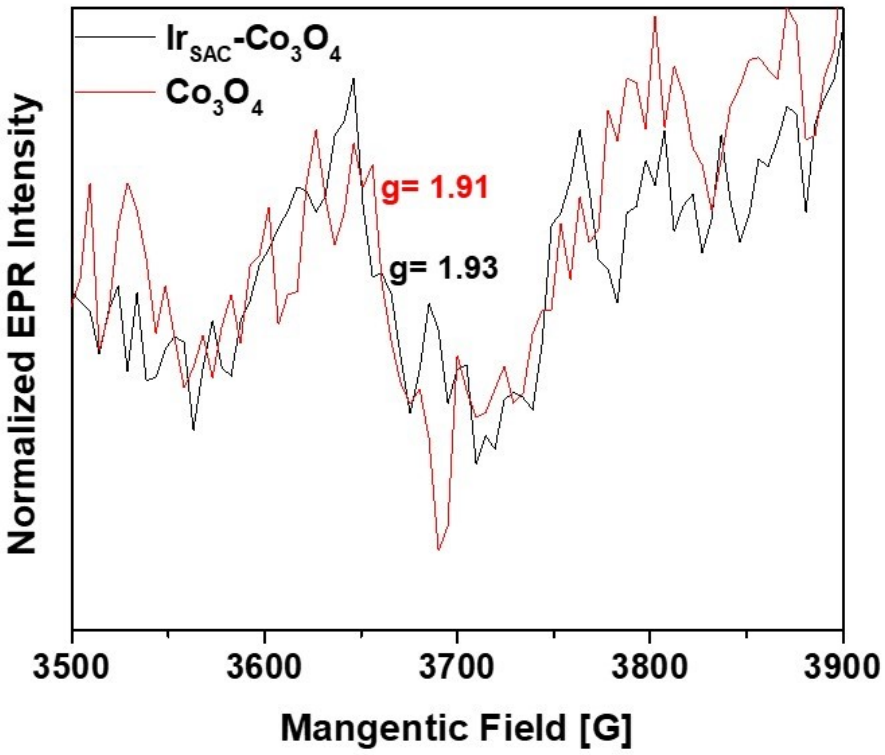

Figure S6: OER activity of other samples synthesized with various amount of $IrCl_3$ and respective onset potentials:

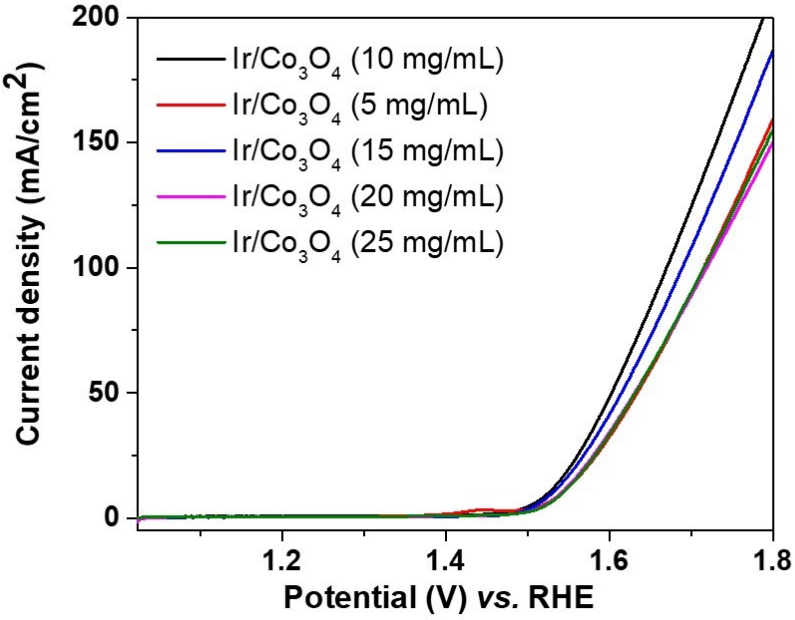

Electrode	Potential (V) *vs.* RHE to generate a current density of 10 mA/cm^2
Ir/Co_3O_4 (5 mg/mL)	1.543
Ir/Co_3O_4 (10 mg/mL)	1.514
Ir/Co_3O_4 (15 mg/mL)	1.531
Ir/Co_3O_4 (20 mg/mL)	1.541
Ir/Co_3O_4 (25 mg/mL)	1.544

Figure S7: (a) CV analysis for Co_3O_4, (b) Ir_{SAC}-Co_3O_4, ECSA analysis of (c) Co_3O_4, and Ir_{SAC}-Co_3O_4sample

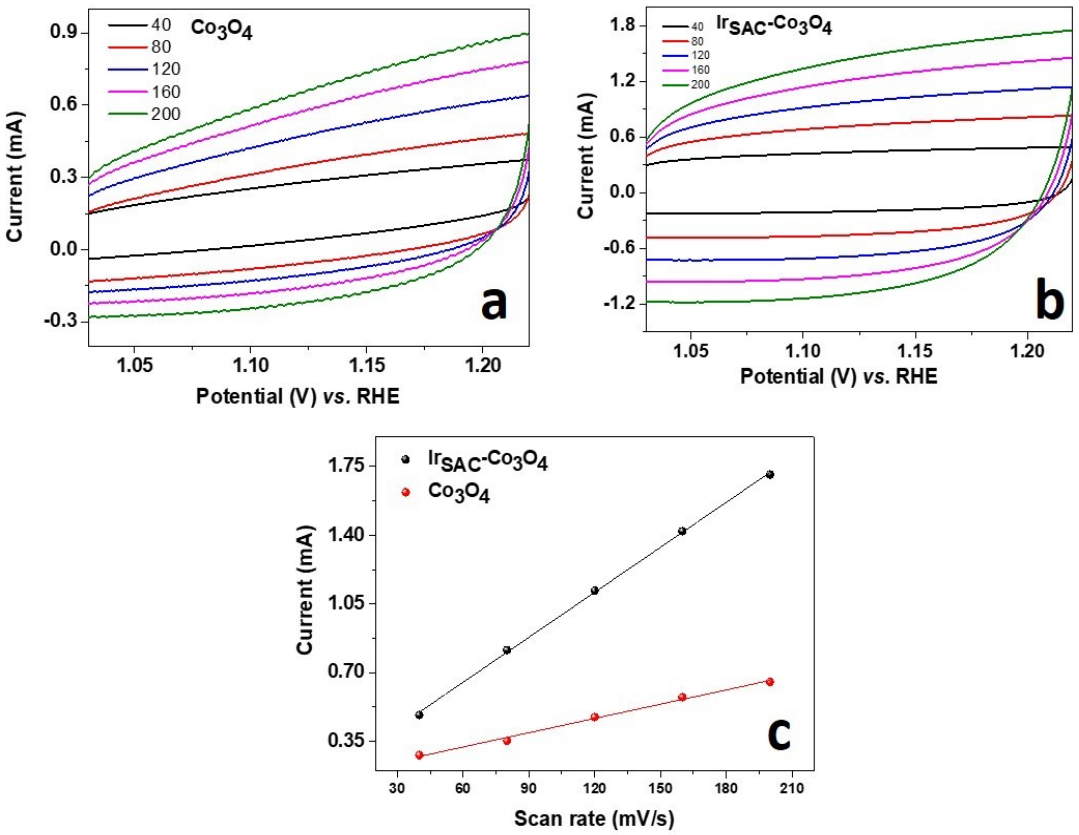

Figure S8: (a) CV analysis for pristine and Ir_{SAC}-Co_3O_4 sample

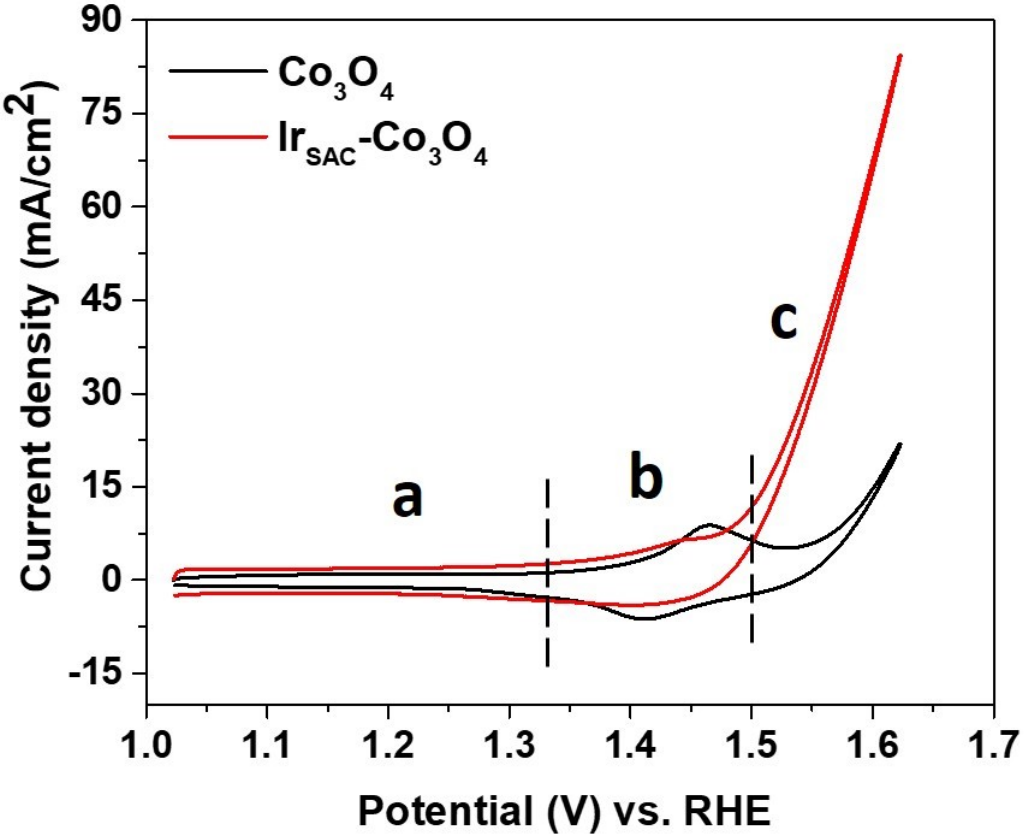

a: -OH + * ⟷ *OH;

b: 2 *OH + Co^{+2} ⟷ Co^{3+}—O* + H_2O;

c: Co^{+3}—O* + $2OH^-$ ⟷ Co^{3+}—O* + O_2

Figure S9: Post electrocatalysis FESEM analysis of Ir_{SAC}-Co_3O_4

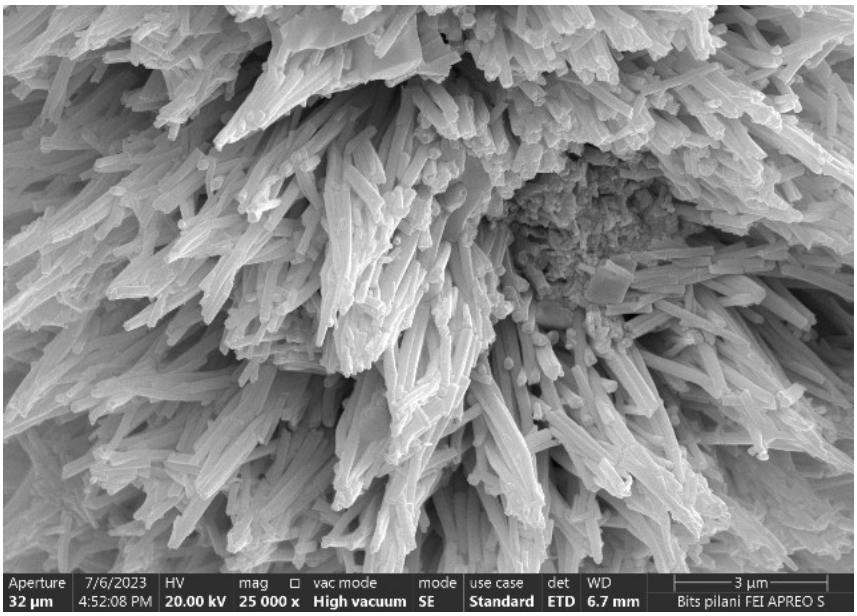
Aperture
32 µm
7/6/2023
4:52:08 PM
HV
20.00 kV
mag
25 000 x
vac mode
High vacuum
mode
SE
use case
Standard
det
ETD
WD
6.7 mm
3 µm
Bits pilani FEI APREO S

Figure S10: Post electrocatalysis XPS analysis of Ir_{SAC}-Co_3O_4 (a) survey spectra, deconvoluted spectra of (b) O 1s, (c) Co 2p

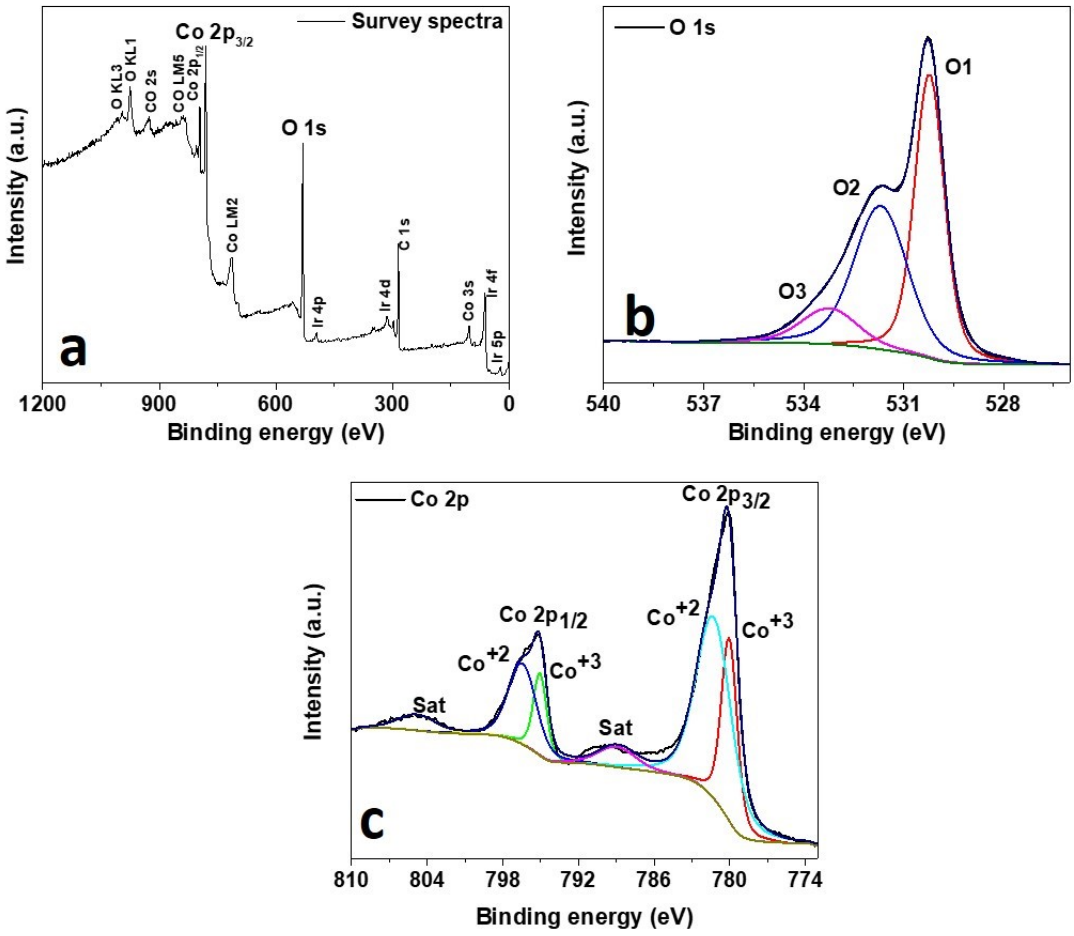

Figure S11: Raman analysis of Co_3O_4 and Ir_{SAC}-Co_3O_4 sample for Pre and post electrocatalysis

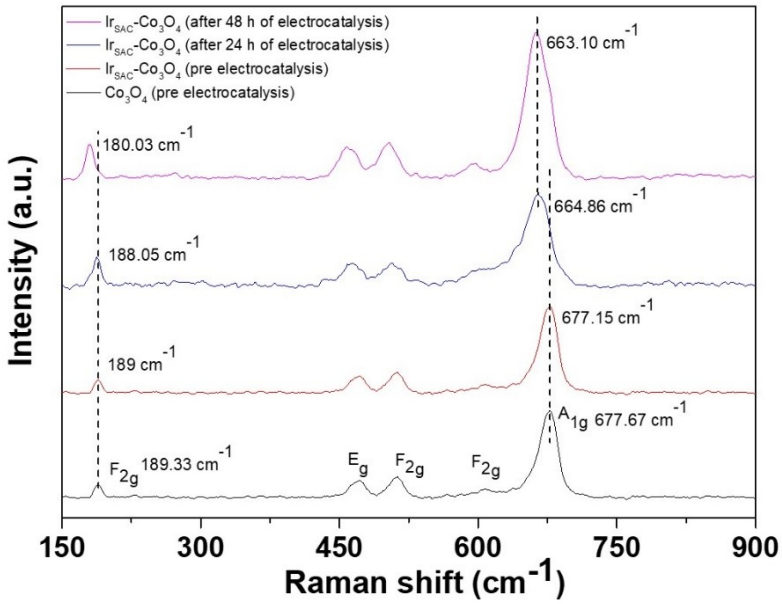

Figure S12: Post electrocatalysis XRD analysis of Ir_{SAC}-Co_3O_4 F

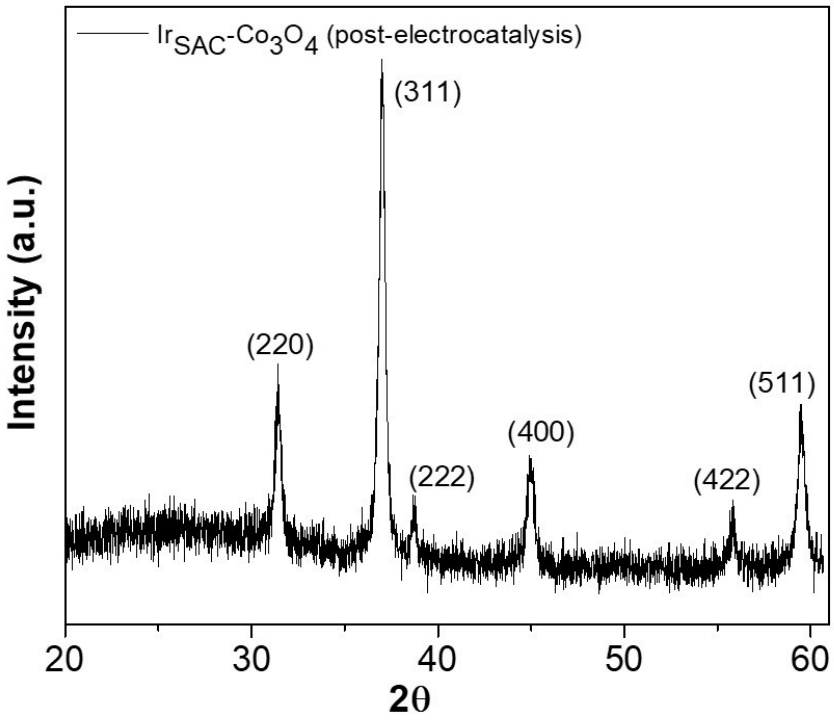

Figure S13. Optimized crystal structures of **(a)** pristine and **(b)** O-vacant Co_3O_4 systems as attained from the DFT calculations.

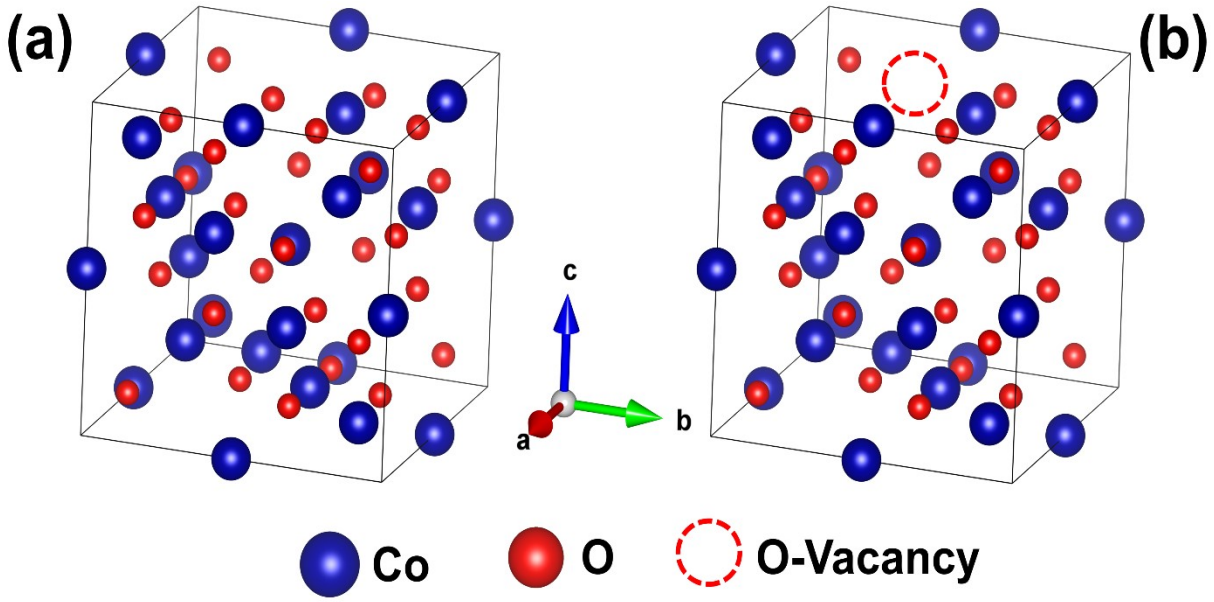

References:

1. B. Ravel and M. Newville, *Synchrotron Radiation*, 2005, **12**, 537-541.
2. B. Ravel, *Synchrotron Radiation*, 2001, **8**, 314-316.
3. P. Giannozzi, O. Baseggio, P. Bonfà, D. Brunato, R. Car, I. Carnimeo, C. Cavazzoni, S. de Gironcoli, P. Delugas, F. Ferrari Ruffino, A. Ferretti, N. Marzari, I. Timrov, A. Urru and S. Baroni, *J. Chem. Phys.*, 2020, **152**, 154105.
4. P. Giannozzi, O. Andreussi, T. Brumme, O. Bunau, M. Buongiorno Nardelli, M. Calandra, R. Car, C. Cavazzoni, D. Ceresoli, M. Cococcioni, N. Colonna, I. Carnimeo, A. Dal Corso, S. de Gironcoli, P. Delugas, R. A. DiStasio, A. Ferretti, A. Floris, G. Fratesi, G. Fugallo, R. Gebauer, U. Gerstmann, F. Giustino, T. Gorni, J. Jia, M. Kawamura, H. Y. Ko, A. Kokalj, E. Küçükbenli, M. Lazzeri, M. Marsili, N. Marzari, F. Mauri, N. L. Nguyen, H. V. Nguyen, A. Otero-de-la-Roza, L. Paulatto, S. Poncé, D. Rocca, R. Sabatini, B. Santra, M. Schlipf, A. P. Seitsonen, A. Smogunov, I. Timrov, T. Thonhauser, P. Umari, N. Vast, X. Wu and S. Baroni, *J. Phys.: Condens. Matter*, 2017, **29**, 465901.
5. P. Giannozzi, S. Baroni, N. Bonini, M. Calandra, R. Car, C. Cavazzoni, D. Ceresoli, G. L. Chiarotti, M. Cococcioni, I. Dabo, A. Dal Corso, S. de Gironcoli, S. Fabris, G. Fratesi, R. Gebauer, U. Gerstmann, C. Gougoussis, A. Kokalj, M. Lazzeri, L. Martin-Samos, N. Marzari, F. Mauri, R. Mazzarello, S. Paolini, A. Pasquarello, L. Paulatto, C. Sbraccia, S. Scandolo, G. Sclauzero, A. P. Seitsonen, A. Smogunov, P. Umari and R. M. Wentzcovitch, *J. Phys.: Condens. Matter*, 2009, **21**, 395502.
6. D. F. Shanno, *Math. Comp.*, 1970, **24**, 647-656.
7. D. Goldfarb, *Math. Comp.*, 1970, **24**, 23-26.
8. R. Fletcher, *Comput. J.*, 1970, **13**, 317-322.
9. C. G. Broyden, *IMA J. Appl. Math.*, 1970, **6**, 76-90.
10. A. Dal Corso, *Comput. Mater. Sci.*, 2014, **95**, 337-350.
11. J. P. Perdew, A. Ruzsinszky, G. I. Csonka, O. A. Vydrov, G. E. Scuseria, L. A. Constantin, X. Zhou and K. Burke, *Phys. Rev. Lett.*, 2008, **100**, 136406.
12. D. Rathore, S. Ghosh, A. Gupta, J. Chowdhury and S. Pande, *ACS Appl. Nano Mater.*, 2024, **7**, 9730-9744.
13. D. Rathore, S. Ghosh, J. Chowdhury and S. Pande, *ACS Appl. Nano Mater.*, 2023, **6**, 3095-3110.
14. D. Rathore, S. Ghosh, J. Chowdhury and S. Pande, *ACS Appl. Nano Mater.*, 2022, **5**, 11823-11838.
15. C. Freysoldt, B. Grabowski, T. Hickel, J. Neugebauer, G. Kresse, A. Janotti and C. G. Van de Walle, *Rev. Mod. Phys.*, 2014, **86**, 253-305.
16. S. Lany and A. Zunger, *Phys. Rev. B*, 2008, **78**, 235104.
17. J. Heyd, G. E. Scuseria and M. Ernzerhof, *J. Chem. Phys.*, 2003, **118**, 8207-8215.
18. C. Lin, Y. Zhao, H. Zhang, S. Xie, Y.-F. Li, X. Li, Z. Jiang and Z.-P. Liu, *Chem. Sci.*, 2018, **9**, 6803-6812.
19. Q. Wang, X. Huang, Z. L. Zhao, M. Wang, B. Xiang, J. Li, Z. Feng, H. Xu and M. Gu, *J. Am. Chem. Soc.*, 2020, **142**, 7425-7433.
20. M.-Q. Yang, K.-L. Zhou, C. Wang, M.-C. Zhang, C.-H. Wang, X. Ke, G. Chen, H. Wang and R.-Z. Wang, *J. Mater. Chem. A*, 2022, **10**, 25692-25700.

21. A. Kumar, M. Gil-Sepulcre, J. P. Fandré, O. Rüdiger, M. G. Kim, S. DeBeer and H. Tüysüz, *J. Am. Chem. Soc.*, 2024, **146**, 32953-32964.
22. C.-Z. Yuan, S. Wang, K. San Hui, K. Wang, J. Li, H. Gao, C. Zha, X. Zhang, D. A. Dinh and X.-L. Wu, *Acs Catal.*, 2023, **13**, 2462-2471.
23. P. Li, M. Wang, X. Duan, L. Zheng, X. Cheng, Y. Zhang, Y. Kuang, Y. Li, Q. Ma and Z. Feng, *Nat. Commun.*, 2019, **10**, 1711.
24. J. Yin, J. Jin, M. Lu, B. Huang, H. Zhang, Y. Peng, P. Xi and C.-H. Yan, *J. Am. Chem. Soc.*, 2020, **142**, 18378-18386.
25. J. Shan, C. Ye, S. Chen, T. Sun, Y. Jiao, L. Liu, C. Zhu, L. Song, Y. Han and M. Jaroniec, *J. Am. Chem. Soc.*, 2021, **143**, 5201-5211.
26. B. Wang, J. Li, D. Li, J. Xu, S. Liu, Q. Jiang, Y. Zhang, Z. Duan and F. Zhang, *Adv. Mater.*, 2024, **36**, 2305437.
27. X. Duan, X. Yu, T. Yang, E. Wang, Y. Hou and X. Hou, *Small*, 2025, **21**, 2503136.
28. J. Chen, Z. Xie, C. Guo, X. Zhou, X. Wang and Z. Tang, *J. Mater. Chem. A*, 2026, **14**, 2931-2937.
29. A. Kumar, M. Gil-Sepulcre, J. Lee, V. Q. Bui, Y. Wang, O. Rüdiger, M. G. Kim, S. DeBeer and H. Tüysüz, *Adv. Mater.*, 2024, **36**, 2401648.
30. J. Wei, H. Tang, L. Sheng, R. Wang, M. Fan, J. Wan, Y. Wu, Z. Zhang, S. Zhou and J. Zeng, *Nat. Commun.*, 2024, **15**, 559.